



Technical Note: No impact of alkenone extraction on foraminiferal stable isotope, trace element and boron isotope geochemistry

Jessica G. M. Crumpton-Banks^{1*}, Thomas Tanner^{2*}, Ivan Hernández Almeida², James W. B. Rae¹, Heather Stoll²

5 ¹School of Earth and Environmental Sciences, University of St Andrews, St Andrews, KY16 9AL, U.K.

²Geological Institute, ETH Zürich, 8092 Zürich, Switzerland

Correspondence to: Jess Crumpton-Banks (jgmc@st-andrews.ac.uk) and Thomas Tanner (Thomas.Tanner@erdw.ethz.ch)

*These two authors contributed equally to this project.

Abstract. Recent advances in geochemical techniques mean that several robust proxies now exist to determine the past
10 carbonate chemistry of the oceans. Foraminiferal $\delta^{11}\text{B}$ and alkenone carbon isotopes allow us to reconstruct sea-surface pH
and pCO_2 respectively, and the ability to apply both proxies to the same sediment sample would give strongly paired datasets
and reduce sample waste. However, no studies to date have examined whether the solvents and extraction techniques used to
prepare alkenones for analysis also impact the geochemistry of foraminifera within those sediments. Here we examine six
15 species pairs of planktic foraminifera, with half being taken from non-treated sediments and half being taken from sediments
where alkenones have been extracted. We look for visual signs of contrasting preservation and compare analyses of $\delta^{18}\text{O}$, $\delta^{13}\text{C}$,
 $\delta^{11}\text{B}$ and trace elements (Li, B, Na, Mn, Mg, Sr, and U/Ca). We find no consistent geochemical offset between the treatments,
and excellent agreement in $\delta^{11}\text{B}$ measurements between them. Our results show that boron isotope reconstructions of pH in
foraminifera from alkenone-extracted sediments can be applied with confidence.

1 Introduction

20 Deep ocean sediment cores provide a wealth of proxy systems for reconstructing Earth's past climate and marine environments.
However, obtaining sediment cores is laborious and expensive, and the recovered material is limited and under increasing
demand for various complementary proxy analyses, at ever increasing resolution. Consequently, it is important to devise
efficient strategies for use of limited core material for multiple proxy systems. Common, widely applied proxy analyses include
(a) high resolution stable isotope analysis on benthic and planktic foraminifera, (b) extraction of lipids such as alkenones and
25 glycerol dialkyl glycerol tetraether (GDGT) lipids for sea surface temperature (SST) reconstruction and for carbon isotopic
determination of alkenones as a pCO_2 proxy, and (c) measurement of foraminiferal trace element chemistry and boron isotopes
to reconstruct SST, pH and pCO_2 .

Conventionally, analysis of organic proxies has been made on separate subsamples of core material than that used for the
analysis of carbonate proxies. However, it would be ideal to obtain proxy information from the same core depth interval, not



30 only to conserve limited core sample but also to improve intercomparison among proxies. In particular, there is benefit to co-
sampling for marine carbonate system proxies, including boron isotopes ($\delta^{11}\text{B}$) in marine carbonates and photosynthetic carbon
isotope fractionation in alkenones (ϵ_p) (Hemming & Hanson, 1992; Rae et al., 2021; Pagani, 2014). Each of these proxies has
its limitations: for example, the 10 Myr residence time of boron in seawater presents a challenge for determining absolute
ocean pH values on multi-millennial timescales (Lemarchand et al., 2002; Foster & Rae, 2016), while phytoplankton-based
35 proxies may struggle to capture low- CO_2 conditions (Badger et al., 2019, Stoll et al., 2019). Furthermore, each of these proxies
solves for only one component of the carbonate system; combining pH and pCO_2 offers us the chance to constrain the carbonate
system more fully than we would be able to from either proxy alone (Rae et al., 2021).

Here we evaluate a sample protocol which first extracts lipids from freeze-dried sediment cores, and subsequently isolates the
coarse (foraminifera) and fine carbonate for stable isotope, trace element, and boron isotope analysis. We assess whether the
40 high temperature solvent extraction used for lipid extraction impacts foraminifera geochemistry, either through leaching or
through contamination which is not removed during the cleaning process. We analysed samples of several species of planktic
foraminifera which were split into pairs, where half of each sediment sample had been treated for total lipid extraction by
solvents (Accelerated Solvent Extraction, ASE), and half were untreated. We examined the preservation of the specimens
using scanning electron microscope (SEM), and analysed several geochemical parameters ($\delta^{18}\text{O}$, $\delta^{13}\text{C}$, trace element ratios
45 and $\delta^{11}\text{B}$) to assess whether foraminifera geochemistry is affected by the solvent extraction.

2 Material and methods

Sediment samples (Table 1) were selected from 3 core sites: Ocean Drilling Program (ODP) Hole 926B from the Ceara Rise
in the western equatorial Atlantic ($3^\circ 43'\text{N}$, $42^\circ 54'\text{W}$, 3598 m), with one sediment sample being taken from 20H5-141-145 cm
(age 7.95 Ma from Wilkens et al., 2017); Integrated Ocean Drilling Program (IODP) Site U1406, south of Newfoundland in
50 the North Atlantic ($40^\circ 21'\text{N}$, $51^\circ 39'\text{W}$, 3814 m), with one sediment sample taken from Hole U1406B (sample depth 8H6 8-
12; age 22.43 Ma van Peer, 2017); and ODP Site 1168, off the southeast coast of Tasmania ($43^\circ 37'\text{S}$, $114^\circ 25'\text{E}$, 2463 m;
where two sediment samples were taken, one from 25X4 50-52 and one from 26X4 50-52; rough age estimate of 13.5 Ma from
Stickley et al., 2004). Sediment samples were then split into 2 parts, with one half being treated to extract alkenones (ASE
treated), and both halves subsequently washed with Milli-Q water (MQ) to process the $> 150\ \mu\text{m}$ size fraction for picking.

55

2.1 Solvent extraction of lipids

Freeze-dried sediment was extracted using a Thermo Dionex 350 accelerated solvent extractor at the Department of Earth
Sciences of ETH Zürich, with a 5:1 ratio of dichloromethane to methanol ($\text{CH}_2\text{Cl}_2/\text{MeOH}$) in three static cycles at 100°C .
Subsequently, sediment was sieved with deionized water through a $150\ \mu\text{m}$ sieve and oven dried overnight at 50°C .



60 **Table 1. Core ID, age, species and mass picked for geochemical analyses. Note that samples were initially counted and weighed prior to ultrasonic tests and mounting for SEM analysis; further specimens were subsequently picked for *T. trilobus* and *G. miotumida*. Final numbers analysed were determined from light images taken just prior to crushing and are given in square brackets. ¹Wilkins et al. (2017) ²van Peer (2017), ³Stickley et al. (2004).**

Core	Age (Mya)	Species	Treatment	Number weighed [analysed]	Mass (mg)
926B-20H5-141	7.95 ¹	<i>T. trilobus</i>	Pre-ASE	74 [88]	2.12
926B-20H5-141	7.95 ¹	<i>T. trilobus</i>	ASE	51 [108]	2.50
926B-20H5-141	7.95 ¹	<i>G. menardii</i>	Pre-ASE	110 [105]	1.61
926B-20H5-141	7.95 ¹	<i>G. menardii</i>	ASE	130 [128]	2.27
1406-8H 8-12	22.43 ²	<i>D. venezuelana</i>	Pre-ASE	85 [83]	1.72
1406-8H 8-12	22.43 ²	<i>D. venezuelana</i>	ASE	75 [73]	1.99
189-1168A-26X-4 50-52	13.5 ³	<i>D. venezuelana</i>	Pre-ASE	27 [20]	1.74
189-1168A-26X-4 50-52	13.5 ³	<i>D. venezuelana</i>	ASE	34 [28]	2.17
189-1168A-25X-4 50-52	13.0 ³	<i>O. universa</i>	Pre-ASE	15 [13]	0.42
189-1168A-25X-4 50-52	13.0 ³	<i>O. universa</i>	ASE	17 [16]	0.35
189-1168A-25X-4 50-52	13.0 ³	<i>G. miotumida</i>	Pre-ASE	31 [43]	0.49
189-1168A-25X-4 50-52	13.0 ³	<i>G. miotumida</i>	ASE	53 [54]	0.61

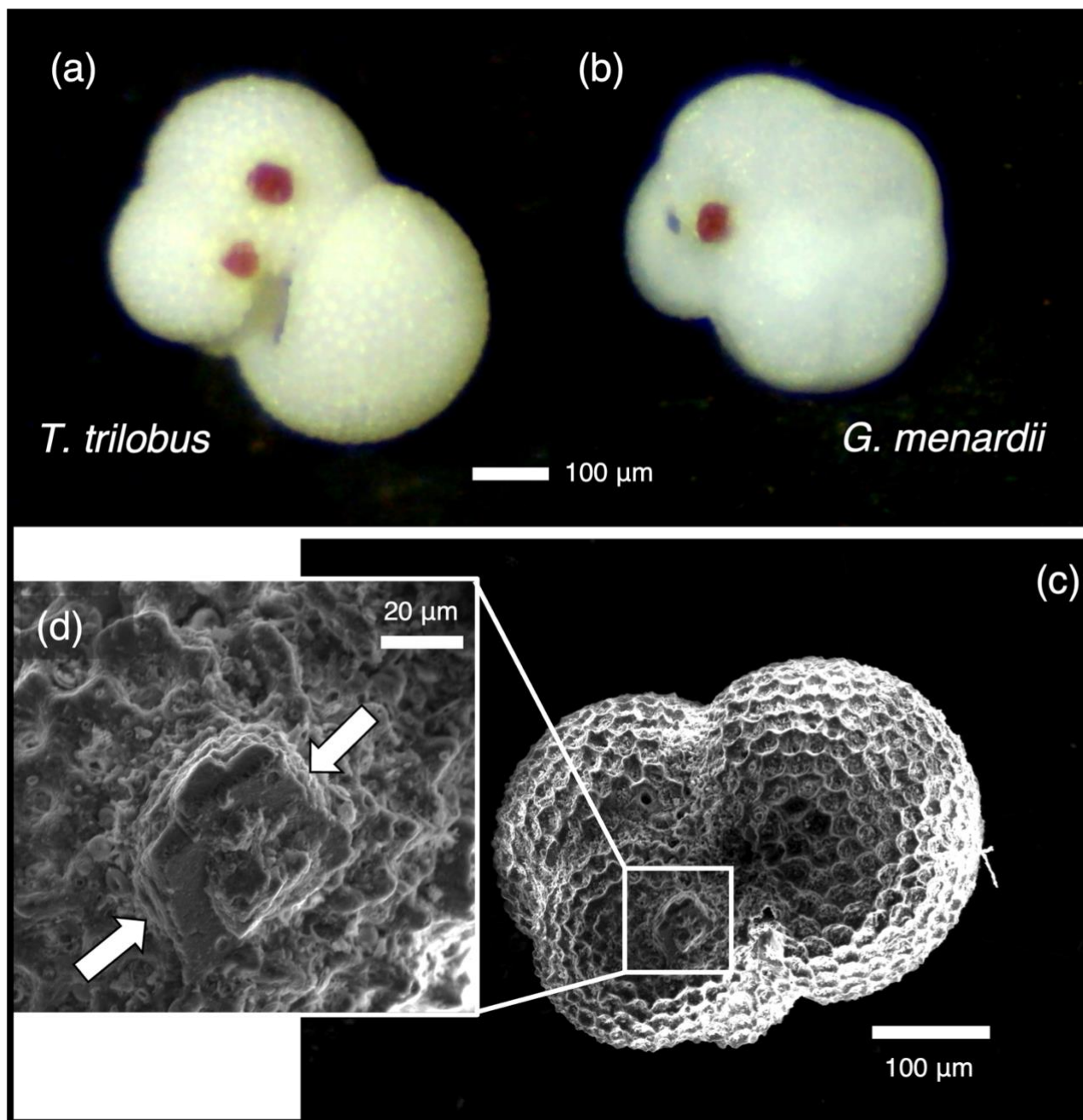
65 2.2. Preparation of foraminifera samples

Several planktic foraminifera species from the > 150 µm size fraction were picked across both sediment treatments: from core 926B, *Trilobatus trilobus* and *Globorotalia menardii*, from core 1406B *Dentoglobigerina venezuelana*, and from 1168A, *Dentoglobigerina venezuelana*, *Orbulina universa* and *Globorotalia miotumida*. These include species which secrete a crust (*D. venezuelana*) as well as thinner walled species which consist of ontogenetic calcite without a crust (*T. trilobus*, *G.*

70 *miotumida*, *O. universa*).

Some foraminifera of both *T. trilobus* and *G. menardii* from core 926B exhibited dark pink crystalline growths on their surface (Fig. 1). Samples were weighed prior to analysis, with sample mass falling between 0.35 – 2.50 mg (Table 1). *O. universa* and *G. miotumida* from core 1168A were sample limited, with less than 1 mg of sample available for each treatment of these species. Between 1 – 3 individuals from each sample were mounted for SEM. The remaining specimens were imaged using a

75 light microscope and counted, and then gently crushed between 2 glass slides, with the pink crystals in samples from core 926B being removed by hand at this stage, and the samples then homogenized.



80 Fig 1. Crystal overgrowths on samples from ODP 926B, possibly a host phase for the anomalously high Mn ($> 400 \mu\text{mol/mol Mn/Ca}$) observed in these samples. Identified on non-treated and ASE-treated specimens of *T. trilobus* (a) and b) *G. menardii*. c) SEM image of ASE-treated *T. trilobus* with crystalline overgrowth shown in white box and d) identified by white arrows.



2.2 SEM assessment of preservation

85 To enable assessment of structural integrity, samples for SEM analysis were gently cracked open using a metal stylus. Fragments were mounted on carbon tape with the broken side facing upwards and were carbon coated. Backscatter electron imaging was carried out on a JSM-IT200 at the University of St Andrews, with accelerating voltages of 10 kV or 15 kV. Visual assessment mainly focused on the cross-section of foraminiferal tests, where the presence or absence of structural features and calcite texture can be strong indicators of overall preservation.

90

2.3 Foraminiferal geochemistry

2.3.1 Stable isotopes ($\delta^{13}\text{C}$ and $\delta^{18}\text{O}$)

A small aliquot (~0.2 mg) of the same crushed sample prepared for trace elements and boron isotopes was used for stable isotope analysis. This aliquot was rinsed twice with deionized water and once with MeOH and dried overnight at 50°C.

95 Samples were analysed at ETH Zurich on a GAS BENCH II system coupled to a Delta V Plus irMS (Thermo Scientific) following procedures described by Breitenbach and Bernasconi (2011). Analytical precision after system calibration by two in-house standards and international standards NBS-19 and NBS-18 was 0.07‰ for both stable isotopes. Values are reported relative to the VPDB standard.

2.3.2 Foraminiferal cleaning

100 All cleaning prior to dissolution and subsequent sample handling was carried out in class 100 clean facilities at the University of St Andrews. Boron-free MQ water was used throughout cleaning and analysis. HNO_3 and HCl acids used were distilled in-house and were of equivalent cleanliness to ultrapure acid. All plastics were subject to acid-cleaning procedures before use. Prior to analysis, foraminiferal samples were mechanically and chemically cleaned to remove clays and organic matter. Mn-Fe oxides may be removed using a reductive clean, but this has been found to notably impact trace element ratios including

105 Mg/Ca (Barker et al., 2003) and so we exclude this step. The cleaning protocol used here follows that of Barker et al. (2003), with some modifications. Initial tests on samples from 1168A found that single specimens *O. universa* and *G. miotumida* were damaged by a few seconds of ultrasonic cleaning and due to this, the ultrasonic time used in each cleaning step was reduced from 30 s to 5 s. The thicker tests of *D. venezuelana* did not show visual signs of damage, but to ensure consistency across samples, all clay-cleaning and oxidation ultrasonic steps were shortened. Al/Ca was measured at < 25 $\mu\text{mol/mol}$ for all samples,

110 indicating that this was an adequate time to remove all clay contamination. Samples were suspended in a small volume (~50 μL) of MQ in a microcentrifuge tube, placed in an ultrasonic bath for 5 s, and clays were removed by adding and then removing ~500 μL MQ. These clay removal steps were repeated for a total of five times. To remove organic contaminants, 250 μL of 1 % H_2O_2 solution buffered with 0.1 M NH_4OH was added to the samples, which were then placed in an 80 °C water bath for 5 minutes. Samples were removed from the water bath, opened to release pressure, and then placed in an ultrasonic bath for 5 s.



115 These steps were repeated three times, with the exception of the smaller mass samples: *O. universa* samples were not given
the oxidative ultrasonication, and *G. miotumida* samples were only given one oxidative ultrasonic step. The oxidative solution
was then diluted with MQ, removed, and the foraminifera fragments were rinsed a further two times. Samples were transferred
to new acid-cleaned vials, and a weak acid leach of 250 μL 0.0005 M HNO_3 was applied for 30 s before being removed and
samples being rinsed three times with MQ. Samples were dissolved in 100 μL MQ and 40 μL 0.5 M HNO_3 , with additional
120 20 μL aliquots of 0.5 M HNO_3 being used to aid dissolution as required. Samples were then transferred into Teflon or plastic
vials and Parafilm[®] prior to trace element and boron isotope analysis.

2.3.3 Trace metal analysis

Trace element ratios of the dissolved samples were analysed by QQQ ICP-MS at the University of St Andrews. Ca, Li, B, Na,
Mg, Al, Mn, Sr and U were measured. An in-house trace element standard (BSGS spiked with NIST RM 951) was used to
125 bracket samples and consistency standards. A small (3 μL) aliquot of sample was diluted and analysed for Ca concentration;
these results were used to dilute samples and standards to a consistent [Ca] matrix of 1 mM. In-house consistency standards
CS1, CS2 and CS3, as well as NIST RM 8301F (Stewart et al., 2021), were measured before and during the run. Reproducibility
of 8301F ($n = 5$) is as follows: Li/Ca 2.42 %, B/Ca 0.93 %, Na/Ca 2.36 %, Mg/Ca 0.89 %, Al/Ca 2.73 %, Mn/Ca 0.68 %, Sr/Ca
0.43 % and U/Ca 1.58 %. For B/Ca we also report the uncertainty on CS3 (3.02 %), which is closer in B/Ca (40 $\mu\text{mol/mol}$) to
130 that of the samples (41 – 79 $\mu\text{mol/mol}$ B/Ca). All Al/Ca values fell below 25 $\mu\text{mol/mol}$, with 9 out of 12 samples having an
Al/Ca value less than 10 $\mu\text{mol/mol}$, indicating that the dissolved samples were clean of clay contamination.

2.3.4 Boron isotope analysis

Boron isotopes were analysed at the University of St Andrews on a Neptune Plus MC-ICPMS equipped with 10^{13} Ω resistors.
Separation of the sample boron from the carbonate matrix was carried out using columns filled with Amberlite IRA-743 (Kiss,
135 1988) and closely followed the procedure of Foster (2008). Samples were buffered to pH ~6 using ammonium acetate buffer
at 1.5x the volume of acid used for dissolution and eluted in a small volume (9x 50 μL) of 0.5 M HNO_3 to boost the measured
signal. To aid washout and boost signal, eluted samples were spiked with Romil-Spa ultrapure HF to a concentration of 0.3 M
(Rae et al., 2018; Zeebe & Rae, 2020). Total procedural blanks were small (< 10 pg B, $n = 3$), with all procedural blank
corrections applied being < 0.04 %. Sample size and indicator elements for contamination (Na, Ca, Mg), either from remaining
140 carbonate matrix or other sources, were assessed prior to analysis, with no signs of remaining matrix or secondary
contamination identified. Due to differing initial starting masses, sample size was variable, with the lower mass samples of *G.*
miotumida and *O. universa* falling between 0.4 – 1.2 ng B; the remaining samples had 3.7 – 11.8 ng B. For the larger samples,
the sample-standard bracketing approach of Foster (2008) was used. The smaller samples gave low concentrations (< 1.6 ppb
[B]), which can make samples more sensitive to an inaccurate in-sequence blank correction; for this reason, these samples
145 were individually blank-corrected and blocks of four samples were standard-bracketed. The average difference between



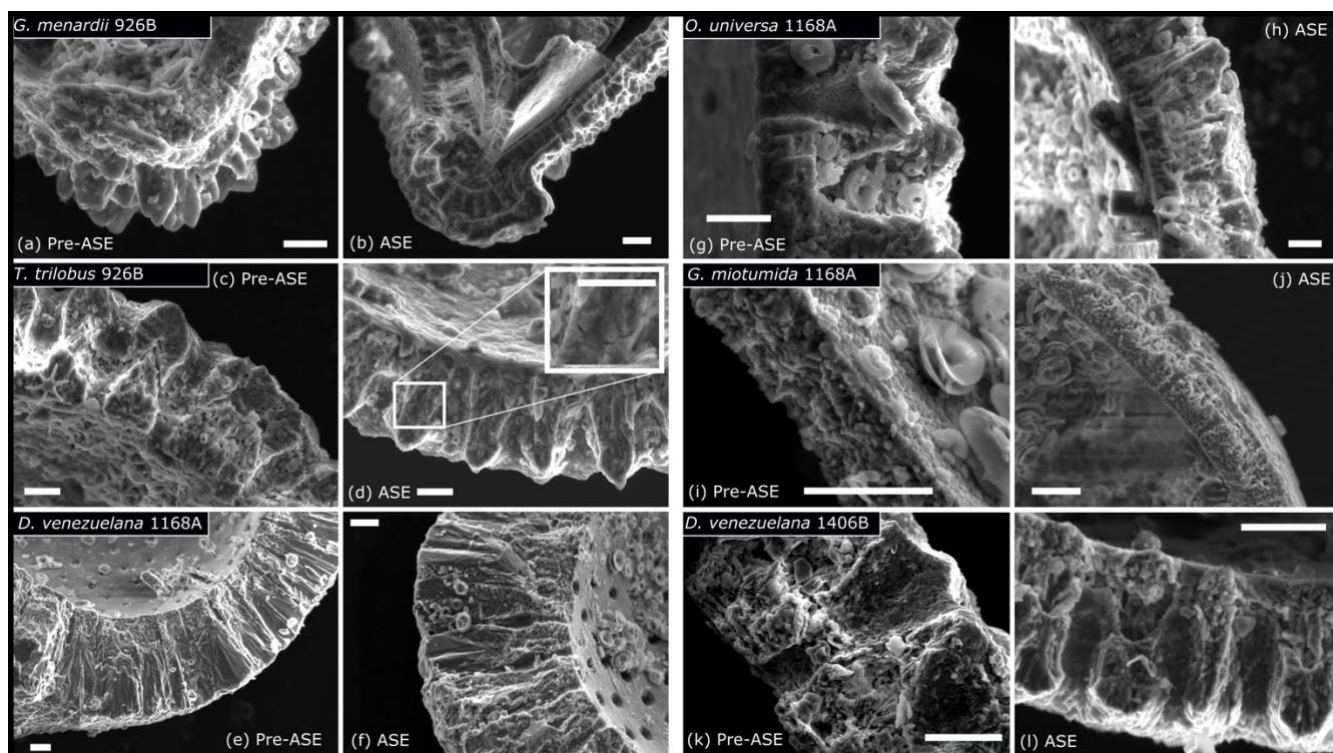
150 bracketing standards for samples analysed in this way was < 0.15 ‰, which is comparable to the main run. NIST RM AE121 (main sequence) reproduced at 19.66 ± 0.17 ‰, and the in-house standard BIG-D reproduced at 14.82 ± 0.13 ‰ (main sequence, 10 ppb) and 14.86 ± 0.36 ‰ (small sample sequence, 5 ppb). The procedural standard NIST RM 8301F (Stewart et al., 2021) reproduced at 14.53 ± 0.08 (2SD) ‰ ($n = 7$, 10 ppb). Uncertainty is shown at 2SD equivalent based on the characteristic reproducibility of standards of equivalent size to the samples run here (0.20 ‰ for the main run samples, 0.40 ‰ for the smaller samples). This is likely conservative given that samples in the main run were all run at greater concentrations than the full procedural NIST RM 8301F standard, which was run at 10 ppb and reproduced at 0.08 ‰ (2SD, $n=7$). Due to sample loss, only 1 replicate of ASE-treated *T. trilobus* was carried out, and so a greater uncertainty of 0.35 ‰ was assigned to this sample.

155

3 Results and discussion

3.1 Physical preservation

SEM assessment of the foraminifera finds variable preservation between sites and species (Fig. 2), but little difference in preservation between treatments. The exception to this is in both pairs of samples from 926B, where foraminifera from the ASE-treated sediments possibly appear slightly better preserved than the non-treated samples. Fine laminations are better preserved in ASE-treated *G. menardii* specimens from 926B compared to the non-treated specimens, where broken faces show more signs of etching (a more “ragged” appearance), and in some instances it is difficult to identify the individual layers of calcite or fine features such as the location of the primary organic membrane. *T. trilobus* individuals from 926B show a similar pattern of preservation, with better preservation of fine details through the test in the ASE-treated samples (see inset), while the non-treated samples appear more heavily etched. We also note the lack of structures such as pores visible on the internal surface of the ASE specimen examined, with an accompanying smooth appearance suggesting the presence of an authigenic phase. The remaining pairs from cores 1406B and 1168A show consistent preservation patterns within pairs. *D. venezuelana* specimens from core 1168A exhibits good preservation, with minimal etching, smooth internal test surfaces and smooth calcite crystals faces in the crust calcite. *O. universa* and *G. miotumida* specimens from 1168A show less good preservation, with etched calcite and pits visible in pores, though we note that the internal trochospiral part of the *O. universa* test was intact and visible in both individuals imaged. This discrepancy in preservation between species in the same sample may be due to the presence of a thick dissolution-resistant calcite crust in *D. venezuelana* (Schiebel & Hemleben, 2017; Petró et al., 2018). *D. venezuelana* also has low Mg/Ca compared to many of the other species in this study (see section 3.3), which may further contribute to a higher preservation potential. *D. venezuelana* from core 1406B shows less good preservation than in core 1168A, with etching and pitting visible, likely due to differences in preservation potential between the sites, alongside a lower degree of crusting and slightly higher Mg/Ca.



180 Fig 2. SEM images assessing impact of ASE treatment on microstructural preservation of foraminifera. a) Pre-ASE *G. menardii*
185 from 926B show signs of etching and the loss of fine detail in some samples, while ASE treated specimens (b) have laminations
preserved, although etching across the test wall is present. c) Pre-ASE *T. trilobus* from 926B are also etched, with some rough inner
190 surfaces and the loss of fine features between calcite layers, while these appear better preserved in samples from the ASE treatment,
with the inset showing a higher magnification view of fine cross-sectional structural details (d); though note the loss of pores on the
inner surface of ASE-treated *T. trilobus*, indicating mineral overgrowth. e) *D. venezuelana* from 1168A pre-ASE treated and f) ASE
treated. In both the inner surface is smooth with no etching, and the outer calcite crust is well-preserved. Some slight etching of
laminar calcite visible. g) *O. universa* from 1168A pre-ASE treated and h) ASE treated. Etching visible in test cross section for both,
as well as pitting in pre-ASE pore surface, though inner trochospiral form is preserved in both samples (not shown). i) Pre-ASE
treated *G. miotumida* from core 1168A and j) ASE treated. As for the *O. universa*, etching is visible across the test wall. k) *D.*
190 *venezuelana* from 1406B, pre-ASE treated and l) ASE treated. Etching and pitting visible in both, although fine features such as
layers are preserved. All scale bars shown are 10 μ m.

The potential for better preservation following ASE treatment is unexpected. One possible explanation for the slight differing
preservation between treatments observed in sediment core 926B could be sorption of the solvents used in alkenone extraction
195 to the calcite surface, which might then protect the foraminifera from dissolution due to undersaturation of water used during
sediment washing. We also note that the low number of individuals assessed by SEM for each species treatment (< 3) makes
it possible the discrepancy is due to heterogeneity between specimen preservation. Based on the results of the SEM assessment
of samples, ASE treatment does not appear to negatively impact the preservation of foraminifera hosted in the sediment.



3.2 Stable isotope results

200 The analysis of $\delta^{13}\text{C}$ and $\delta^{18}\text{O}$ across the pairs of treated and non-treated species does not reveal a clear or systematic offset
(Fig. 3, Table 2). The difference in $\delta^{13}\text{C}$ between five out of six pairs is ≤ 0.11 ‰, which falls within 1 SD of each other (with
1 SD being the reported 0.07 ‰ analytical precision). The offset of 0.25 ‰ in the *O. universa* pair is still within 2 SD and is
likely due to the limited sample size (pre-ASE n = 13, ASE n = 16, noting that only a small fraction of this total was used for
stable isotopes following crushing and splitting), rather than any influence of the ASE-treatment.

205

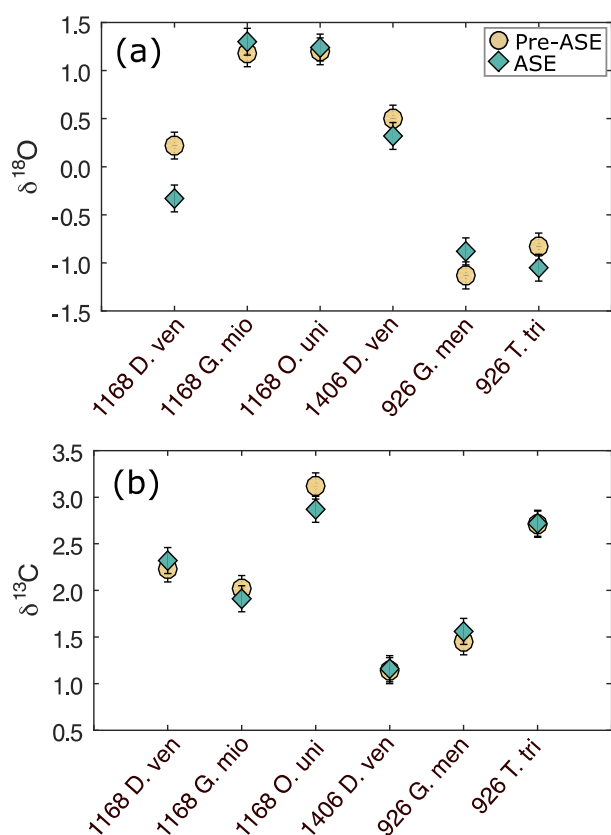


Fig 3. (a) $\delta^{18}\text{O}$ and (b) $\delta^{13}\text{C}$ results for the comparison of pre-ASE (yellow circles) and ASE treated (blue diamonds) foraminifera. Uncertainties are shown as analytical precision of 0.07 ‰. There is no consistent offset between species pairs, supporting the use of stable isotopes in foraminifera from ASE treated sediment.

210



215 **Table 2.** $\delta^{18}\text{O}$, $\delta^{13}\text{C}$ and $\delta^{11}\text{B}$ results for ASE-treated and non-ASE samples. DV = *D. venezuelana*, Mi = *G. miotumida*, Ou = *O. universa*, Men = *G. menardii*, Tt = *T. trilobus*.

Sample	$\delta^{18}\text{O}$ (‰)	1SD (‰)	$\delta^{13}\text{C}$ (‰)	1SD (‰)	$\delta^{11}\text{B}$ (‰)	2SD (‰)
1168Dv	0.22	0.04	2.23	0.01	12.86	0.20
1168Dv-ASE	-0.33	0.03	2.32	0.03	12.98	0.20
1168Mi	1.18	0.05	2.02	0.01	12.70	0.40
1168Mi-ASE	1.30	0.04	1.91	0.04	12.57	0.40
1168Ou	1.20	0.01	3.12	0.03	13.14	0.40
1168Ou-ASE	1.24	0.06	2.87	0.03	13.63	0.40
1406Dv	0.50	0.03	1.14	0.02	14.27	0.20
1406Dv-ASE	0.32	0.04	1.16	0.04	14.38	0.20
926Men	-1.13	0.07	1.45	0.02	16.82	0.20
926Men-ASE	-0.88	0.07	1.56	0.02	16.87	0.20
926Tt	-0.83	0.01	2.71	0.03	17.87	0.20
926Tt-ASE	-1.05	0.05	2.72	0.02	17.66	0.35

The variability among the $\delta^{18}\text{O}$ pairs is in general higher than that for $\delta^{13}\text{C}$, and three pairs have an offset that is larger than 1 SD. *T. trilobus* from 926B and *D. venezuelana* from 1406B have an offset of 0.22 ‰ and 0.18 ‰, respectively, though still fall within 2 SD of the measurement. The only clear outlier is *D. venezuelana* from 1168A with a difference of 0.55 ‰, which after *O. universa* was the second smallest species pair (pre-ASE n = 20, ASE n = 28; and as for *O. universa*, only a small fraction of this crushed sample was analysed for stable isotopes). Therefore interspecimen variability might explain this offset. A species-specific influence cannot entirely be ruled out but seems unlikely since the second pairing of *D. venezuelana* from 1406B is within 2 SD and consisted of up to 4 times the amount of single specimen picked (pre-ASE n = 83, ASE n = 73). These results support the application of $\delta^{13}\text{C}$ and $\delta^{18}\text{O}$ in foraminifera from ASE-treated sediments to be used in palaeoceanographic reconstructions.

3.3 Trace element results

230 There is no consistent offset in trace element ratios between the treatments across the pairs studied (Fig. 4, Table 3). Notably, sample pairs with larger numbers of individuals (*T. trilobus*, *G. menardii* and *D. venezuelana* from 1406B) tend to give values



within analytical error (see Table 1 for specimen counts). More variability is observed in sample pairs with lower numbers of individuals for some elements, which we attribute to heterogeneity between individual specimens.

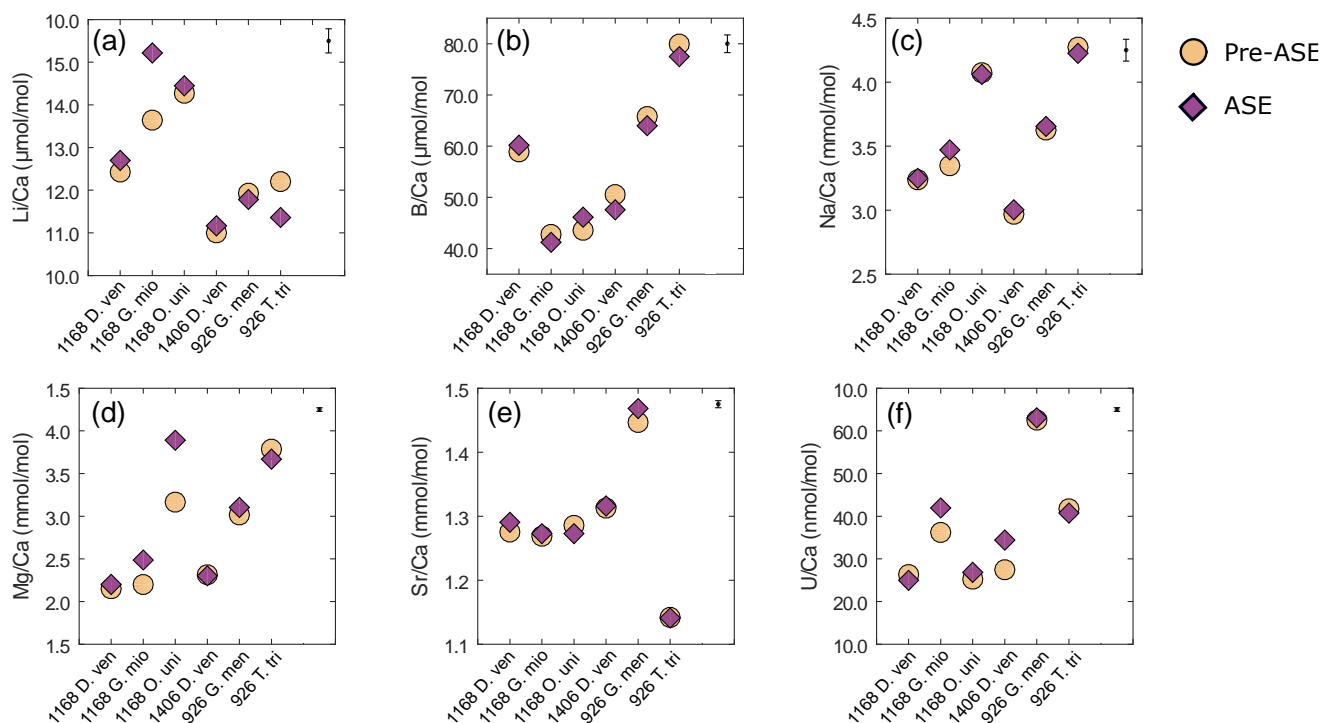


Fig 4. Results of trace element analyses for pre-ASE (yellow circles) and ASE (purple diamonds) for the species from the core sites studied. Uncertainty on the average sample value for each element is shown in the upper right hand corner. No systematic offset is observed between the treatments. (a) = Li/Ca, (b) = B/Ca, (c) = Na/Ca, (d) = Mg/Ca, (e) = Sr/Ca, (f) = U/Ca. D. ven. = *D. venezuelana*, G. mio = *G. miotumida*, O. uni = *O. universa*, G. men = *G. menardii* and T. tri = *T. trilobus*.

235

240

B/Ca ratios were within analytical error for both treatments (Fig. 4). In some cases, small deviations ($< 6\%$) in B/Ca ratios were observed between ASE-treated and untreated samples, but there was no systematic trend of higher or lower B/Ca with ASE treatment. Sr/Ca ratios were not significantly different among treatments for any of the samples examined, with $< 2\%$ variability between all pairs. Similarly, Na/Ca ratios were all within uncertainty, with most pairs exhibiting $< 1.2\%$ variability; *G. miotumida* showed a slightly greater difference with 3.7% difference between the treatments (Fig. 4). In Li/Ca, there is a significant offset of 12.5% observed in Li/Ca for *G. miotumida*, likely attributable to the smaller number of individuals in these samples (pre-ASE $n = 43$, ASE $n = 54$). There is a smaller opposite offset of 7.5% in Li/Ca between treatments for *T. trilobus* which is unlikely to be due to sample size (pre-ASE $n = 88$, ASE $n = 108$). However across the dataset as a whole there is no consistent difference in Li/Ca between treatments.

250



Table 3. Trace element results for ASE-treated and non-ASE samples. DV = *D. venezuelana*, Mi = *G. miotumida*, Ou = *O. universa*, Men = *G. menardii*, Tt = *T. trilobus*.

Sample	Li/Ca μmol mol ⁻¹	B/Ca μmol mol ⁻¹	Na/Ca mmol mol ⁻¹	Mg/Ca mmol mol ⁻¹	Al/Ca μmol mol ⁻¹	Mn/Ca μmol mol ⁻¹	Sr/Ca mmol mol ⁻¹	Cd/Ca nmol mol ⁻¹	Ba/Ca μmol mol ⁻¹	Nd/Ca μmol mol ⁻¹	U/Ca nmol mol ⁻¹
1168Dv	11.43	58.89	3.24	1.64	5.27	70.69	1.28	47.93	6.54	0.33	16.33
1168Dv-ASE	11.70	60.17	3.25	1.69	4.91	68.50	1.29	38.59	6.72	0.32	14.97
1168Mi	12.64	42.76	3.35	1.69	4.51	114.19	1.27	96.01	5.88	0.64	26.21
1168Mi-ASE	14.22	41.22	3.47	1.98	9.53	135.01	1.27	117.39	7.78	0.79	31.94
1168Ou	13.27	43.57	4.07	2.64	7.06	66.58	1.29	39.07	2.34	0.42	15.24
1168Ou-ASE	13.45	46.13	4.06	3.36	5.75	77.58	1.27	44.91	2.83	0.45	16.84
1406Dv	10.00	50.55	2.97	1.79	7.27	762.07	1.31	77.71	2.92	0.94	17.45
1406Dv-ASE	10.17	47.56	3.00	1.79	22.81	984.84	1.32	89.88	4.27	1.27	24.40
926Men	10.93	65.79	3.63	2.49	17.01	842.79	1.45	212.23	6.90	2.43	52.53
926Men-ASE	10.78	63.99	3.65	2.57	8.23	825.24	1.47	197.98	6.10	2.42	53.06
926Tt	11.20	79.94	4.27	3.27	13.23	462.44	1.14	105.72	1.34	1.65	31.74
926Tt-ASE	10.36	77.49	4.22	3.15	7.54	421.90	1.14	93.07	1.36	1.47	30.73

255 Mg/Ca ratios were consistent for samples consisting of a large number of individual foraminifera, which averages out interspecimen variability. In samples with smaller numbers of individuals, specifically the *G. miotumida* and *O. universa* from core 1168A, there were resolvable offsets. Mg is widely observed to be incorporated into foraminiferal laminar calcite in bands, the formation of which has been linked to diurnal processes in planktic foraminifera, including *O. universa* (Eggins et al., 2004; Spero et al., 2015). In contrast crust calcite, such as that exhibited by *D. venezuelana*, tends to lack high-Mg bands and therefore has a lower Mg-content relative to the laminar calcite. While there is an established and robust relationship between foraminiferal Mg/Ca and temperature (Nurnberg, 1995; Elderfield & Ganssen, 2000; Anand et al., 2003; Gray & Evans, 2019), individual foraminifera that have grown in the same environment may record quite different bulk Mg/Ca values from each other (Davis et al., 2017; Davis et al., 2020). This effect may be muted in species with a relatively thick and homogenous crust of low Mg calcite, which may explain the close agreement within pairs for *D. venezuelana* even when the number of specimens analysed is low, as for samples from 1168A (pre-ASE n = 20, ASE n = 28). Given that specimen numbers were limited for *O. universa* (pre-ASE n = 13, ASE n = 16), it is probable that in this case the offset in Mg/Ca values between the treatments is due to interspecimen heterogeneity, rather than any impact of the ASE-treatment. The same process may contribute for the modest number of *G. miotumida* specimens. Similarly, U/Ca is elevated in ASE-treated *G. miotumida* (22 %), *O. universa* (11 %) and slightly reduced in ASE-treated *D. venezuelana* from 1168A (8.4 %). The elevation of 40 % in



270 ASE-treated *D. venezuelana* from 1406B is less likely to be related to specimen number, but may be linked to elevated Mn/Ca
in this sample, discussed below.

Mn/Ca is not notably different between treatments (Fig. 5a), except for *D. venezuelana* from 1406B (ASE sample 29 %
elevated). Regardless of treatment, all species pairs from 1406 (*D. venezuelana*) and 926B (*G. menardii* and *T. trilobus*)
275 showed elevated Mn/Ca values ($> 400 \mu\text{mol/mol}$), which are significantly higher than generally accepted for foraminiferal
samples unaffected by diagenesis (Fig. 5, Table 2). Additional authigenic manganese may accumulate on foraminifera under
changing redox conditions as either Mn-oxides or Mn-carbonates (Boyle, 1981; Boyle, 1983; Morse et al., 2007). Given the
offset in Mn/Ca between *G. menardii* and *T. trilobus* from 926B, but consistency within the pairs, it seems likely that Mn is
hosted in these samples as authigenic Mn-carbonate. This is supported by the absence of internal features such as pores visible
280 in the SEM image of ASE-treated *T. trilobus* (Fig. 2), indicating the precipitation of a secondary mineral phase. The offset
between the species is likely due to differences in Mn/Ca of the host phase caused by either morphology, or initial trace
metal/organic content. Authigenic phases hosting Mn, such as Mn-oxides, may also be enriched in other trace elements
including Mg (Roberts et al., 2012), but we observe no relationship between Mn/Ca and Mg/Ca (Fig 5b; pre-ASE $R^2 = 0.04$,
ASE $R^2 = 0.03$).

285

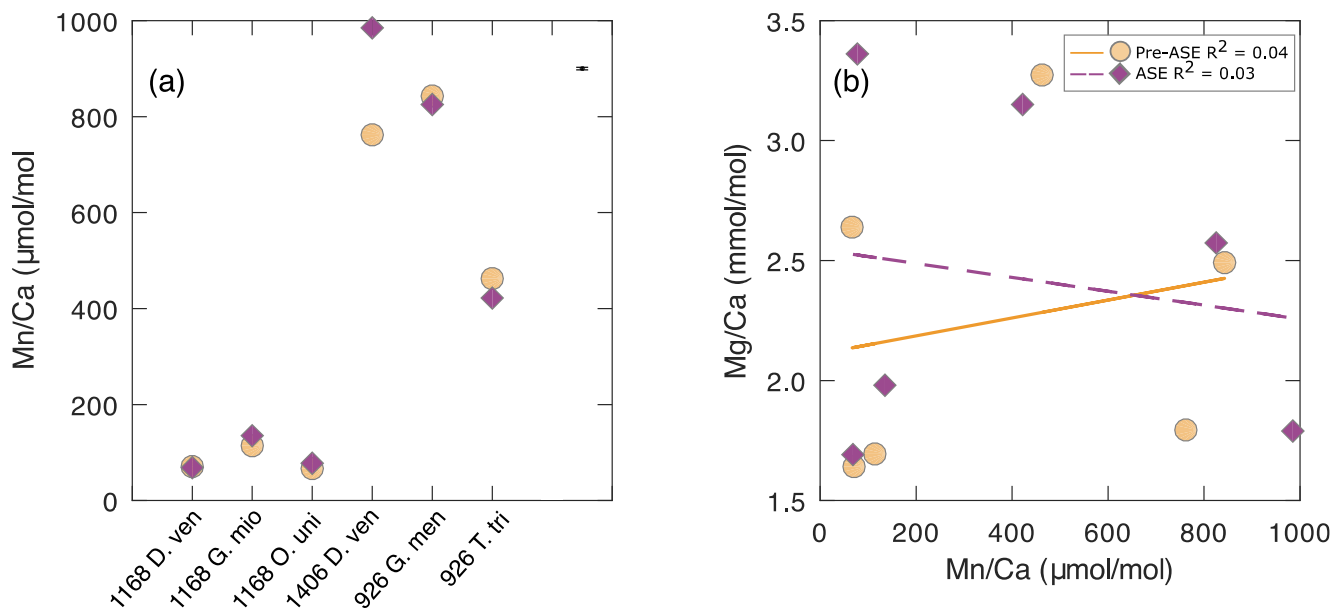


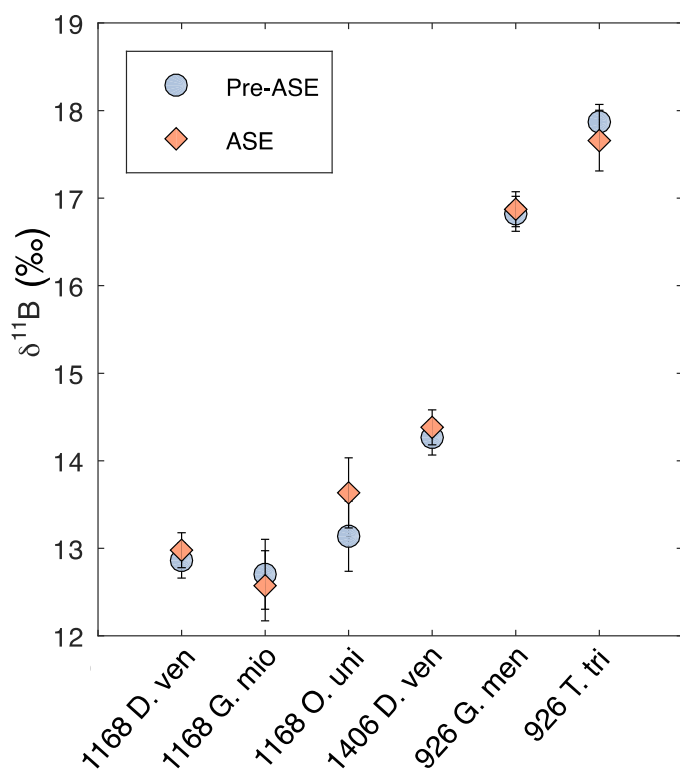
Fig 5. (a) Mn/Ca results for the pre-ASE (yellow circles) and ASE-treated (purple diamonds) foraminifera. (b) There is no discernible
relationship between Mn/Ca and Mg/Ca, indicating that despite high Mn/Ca values indicative of secondary authigenic signals,
foraminiferal Mg/Ca is not affected. Solid yellow line = pre-ASE linear fit, dashed purple line = ASE linear fit.

290



3.4 Boron isotope results

We find no significant difference between the treatments for $\delta^{11}\text{B}$ (Fig. 6, Table 2). In all cases, non-treated and ASE $\delta^{11}\text{B}$ values fall within 2SD of each other. Note that the larger uncertainties for *O. universa* and *G. miotumida* are due to the small mass of these samples. Minor offsets in $\delta^{11}\text{B}$ between different species of planktic foraminifera from the same interval (e.g. 295 between different species in the samples from 1168 and 926) are expected and reflect the combined influence of differences in depth habitat in the water column, and the presence or absence of photosymbionts (Henehan et al., 2016). The positive offsets seen in the trace element measurements of ASE-treated *G. miotumida*, *O. universa* and 1406B *D. venezuelana* are not observed in the boron isotope data. The boron isotope measurements here show no evidence that ASE-treatment impacts foraminiferal $\delta^{11}\text{B}$ and indicate that reconstructions of ocean pH made from ASE-treated foraminifera can be applied with 300 confidence.



305 **Fig 6. Boron isotopes results for comparison of pre-ASE (blue circles) and ASE treated (pink diamonds) foraminifera. No offset between the two treatments is identified, supporting the use of foraminifera from ASE treated sediments for boron isotope reconstructions of pH.**



4 Conclusions

We have undertaken a detailed assessment of the potential impact that ASE treatment of sediments has on the geochemistry and physical preservation of the planktic foraminifera hosted within that sediment. We see no signs that ASE treatment leaches or dissolves foraminiferal calcite and find no evidence that it discernibly influences geochemistry. Some ASE-treated samples do exhibit slightly elevated trace element values, but this is likely due to a small number of individuals analysed. Our findings support the use of foraminifera from ASE-treated sediments for geochemical analyses, including Mg/Ca to reconstruct temperatures, and $\delta^{11}\text{B}$ to reconstruct pH. These findings pave the way for paired $\delta^{11}\text{B}$ and alkenone ε_{p} reconstructions of the carbonate system from the same sediment. We hope that this study will give the scientific community confidence to share ODP samples that might otherwise be discarded as waste and pave the way for new collaborative endeavours.

Data availability: All data from this study is published in the tables within this manuscript.

Author contributions: JCB conducted the SEM preservation study, trace element and boron isotope analyses, interpreted those data, and wrote the first draft of the manuscript. TT conceived and designed the study, procured samples, completed lipid extractions and obtained and interpreted stable isotope analyses. IHA identified and picked foraminifera. All authors contributed to the final manuscript.

The authors declare that they have no conflict of interest.

Acknowledgements

This research was funded by the Swiss National Science Foundation (Award 200021_182070 to HMS) and ETH core funding. JWBR received funding from the European Research Council under the European Union's Horizon 2020 research and innovation program (grant agreement 805246). We acknowledge the support of the EPSRC Light Element Analysis Facility Grant EP/T019298/1 and the EPSRC Strategic Equipment Resource Grant EP/R023751/1, which supported SEM analyses at the University of St Andrews.

References

- Anand, P., Elderfield, H., & Conte, M. H. Calibration of Mg/Ca thermometry in planktonic foraminifera from a sediment trap time series. *Paleoceanography*, 18(2), 1-15, doi:10.1029/2002pa000846, 2003.
- Badger, M. P. S., Chalk, T. B., Foster, G. L., Bown, P. R., Gibbs, S. J., Sexton, P. F. et al. Insensitivity of alkenone carbon isotopes to atmospheric CO_2 at low to moderate CO_2 levels. *Clim Past*, 15(2), 539-554, https://doi.org/10.5194/cp-15-539-2019, 2019.
- Barker, S., Greaves, M., & Elderfield, H. A study of cleaning procedures used for foraminiferal Mg/Ca paleothermometry. *Geochem Geophys Geosy*, 4(9), 1-20, https://doi.org/10.1038/35013033/10.1029/2003gc000559, 2003.



- 340 Boyle, E. A. Cadmium, zinc, copper, and barium in foraminifera tests, 53, 11-35, *Earth Planet Sc Lett*,
[https://doi.org/10.1038/35013033/10.1016/0012-821x\(81\)90022-4](https://doi.org/10.1038/35013033/10.1016/0012-821x(81)90022-4), 1981.
- Boyle, E. A. Manganese carbonate overgrowths on foraminifera tests. *Geochim Cosmochim Ac*, 47(10), 1815-1819,
[https://doi.org/10.1038/35013033/10.1016/0016-7037\(83\)90029-7](https://doi.org/10.1038/35013033/10.1016/0016-7037(83)90029-7), 1983.
- 345 Davis, C. V., Fehrenbacher, J. S., Hill, T. M., Russell, A. D., & Spero, H. J. Relationships Between Temperature, pH, and
Crusting on Mg/Ca Ratios in Laboratory-Grown *Neogloboquadrina* Foraminifera. *Paleoceanography*, 32(11), 1137-
1152, <https://doi.org/10.1038/35013033/10.1002/2017pa003111>, 2017.
- Davis, C. V., Fehrenbacher, J. S., Benitez-Nelson, C., & Thunell, R. C. Trace element heterogeneity across individual
planktic foraminifera from the Modern Cariaco Basin. *J Foram Res*, 50(2), 204-218,
<https://doi.org/10.1038/35013033/10.2113/gsjfr.50.2.204>, 2020.
- 350 Eggins, S., Sadekov, A., & De Dekker, P. Modulation and daily banding of Mg/Ca in tests by symbiont photosynthesis and
respiration: a complication for seawater thermometry. *Earth Planet Sc Lett*, 225(3-4), 411-419,
<https://doi.org/10.1038/35013033/10.1016/j.epsl.2004.06.019>, 2004.
- Elderfield, H., & Ganssen, G. Past temperature and $\delta^{18}\text{O}$ of surface ocean waters inferred from foraminiferal Mg/Ca ratios.
Nature, 405(6785), 442-445, <https://doi.org/10.1038/35013033>, 2000.
- 355 Foster, G. L. Seawater pH, pCO₂ and [CO₂⁻³] variations in the Caribbean Sea over the last 130 kyr: A boron isotope and
B/Ca study of planktic foraminifera. *Earth Planet Sc Lett*, 271(1-4), 254-266, doi: 10.1016/j.epsl.2008.04.015, 2008.
- Foster, G. L., & Rae, J. W. B. Reconstructing Ocean pH with Boron Isotopes in Foraminifera. *Annu Rev Earth Pl Sc*, 44(1),
207-237, <https://doi.org/10.1146/annurev-earth-060115-012226>, 2016.
- 360 Gray, W. R., & Evans, D. Nonthermal influences on Mg/Ca in planktonic foraminifera: A review of culture studies and
application to the last glacial maximum. *Paleoceanography and Paleoclimatology*, 34(3), 306-315,
<https://doi.org/10.1029/2018pa003517>, 2019.
- Hemming, N. G., & Hanson, G. N. Boron isotopic composition and concentration in modern marine carbonates. *Geochim
Cosmochim Ac*, 56(1), 537-543, [https://doi.org/10.1016/0016-7037\(92\)90151-8](https://doi.org/10.1016/0016-7037(92)90151-8), 1992.
- 365 Henehan, M. J., Foster, G. L., Bostock, H. C., Greenop, R., Marshall, B. J., & Wilson, P. A. A new boron isotope-pH
calibration for *Orbulina universa*, with implications for understanding and accounting for 'vital effects'. *Earth Planet
Sc Lett*, 454, 282-292, <https://doi.org/10.1016/j.epsl.2016.09.024>, 2016.
- Kiss, E. Ion-exchange separation and spectrophotometric determination of boron in geological materials. *Anal Chim Acta*,
211, 243-256, [https://doi.org/10.1016/s0003-2670\(00\)83684-3](https://doi.org/10.1016/s0003-2670(00)83684-3), 1988.
- 370 Lemarchand, D., Gaillardet, J., Lewin, E., & Allegre, C. J. Boron isotope systematics in large rivers: implications for the
marine boron budget and paleo-pH reconstruction over the Cenozoic. *Chem Geol*, 190(1-4), 123-140,
[https://doi.org/10.1016/s0009-2541\(02\)00114-6](https://doi.org/10.1016/s0009-2541(02)00114-6), 2002.
- Morse, J. W., Arvidson, R. S., & Lüttge, A. Calcium Carbonate Formation and Dissolution. *Chem Rev*, 107(2), 342-381,
<https://doi.org/10.1002/chin.200719199>, 2007.
- 375 Nürnberg, D. Magnesium in test of *Neogloboquadrina pachyderma* sinistral from high northern and southern latitudes. *J
Foram Res*, 25(4), 350-368, <https://doi.org/10.2113/gsjfr.25.4.350>, 1995.
- Pagani, M. Biomarker-Based Inferences of Past Climate: The Alkenone pCO₂ Proxy. In *Treatise on Geochemistry* (pp. 361-
378). Elsevier, <https://doi.org/10.1016/b978-0-08-095975-7.01027-5>, 2014.
- Petró, S. M., Pivel, M. A. G., & Coimbra, J. C. Foraminiferal solubility rankings: A contribution to the search for consensus.
J Foram Res, 48(4), 301-313, <https://doi.org/10.2113/gsjfr.48.4.301>, 2018.
- 380 Rae, J. W. B., Burke, A., Robinson, L. F., Adkins, J. F., Chen, T., Cole, C. et al. CO₂ storage and release in the deep
Southern Ocean on millennial to centennial timescales. *Nature*, 562(7728), 569-573, <https://doi.org/10.1038/s41586-018-0614-0>, 2018.
- 385 Rae, J. W. B., Zhang, Y. G., Liu, X., Foster, G. L., Stoll, H. M., & Whiteford, R. D. M. Atmospheric CO₂ over the past 66
million years from marine archives. *Annu Rev Earth Pl Sc*, 49, 609-641, <https://doi.org/10.1146/annurev-earth-082420-063026>, 2021.
- Roberts, N. L., Piotrowski, A. M., Elderfield, H., Eglinton, T. I., & Lomas, M. W. Rare earth element association with
foraminifera. *Geochim Cosmochim Ac*, 94, 57-71, <https://doi.org/10.1016/j.gca.2012.07.009>, 2012.
- Schiebel, R., & Hemleben, C. *Planktic foraminifers in the modern ocean*. Springer, <https://doi.org/10.1007/978-3-662-50297-6>, 2017.



- 390 Spero, H. J., Eggins, S. M., Russell, A. D., Vetter, L., Kilburn, M. R., & Hönisch, B. Timing and mechanism for intratest Mg/Ca variability in a living planktic foraminifer. *Earth Planet Sc Lett*, 409, 32-42, <https://doi.org/10.1016/j.epsl.2014.10.030>, 2015.
- Stewart, J. A., Christopher, S. J., Kucklick, J. R., Bordier, L., Chalk, T. B., Dapoigny, A. et al. NIST RM 8301 Boron Isotopes in Marine Carbonate (Simulated Coral and Foraminifera Solutions): Inter-laboratory $\delta^{11}\text{B}$ and Trace Element
395 Ratio Value Assignment. *Geostand Geoanal Res*, 45(1), 77-96, <https://doi.org/10.1111/ggr.12363>, 2021.
- Stickley, C. E., Brinkhuis, H., McGonigal, K. L., Chaproniere, G. C. H., Fuller, M., Kelly, D. C. et al. Late Cretaceous-Quaternary biomagnetostratigraphy of ODP Sites 1168, 1170, 1171 and 1172. *Proceedings of the Ocean Drilling Program, Scientific Results 189*, 1 - 57, <https://doi.org/10.2973/odp.proc.sr.189.111.2004>, 2004.
- 400 Stoll, H. M., Guitian, J., Hernandez-Almeida, I., Mejia, L. M., Phelps, S., Polissar, P. & Ziveri, P. Upregulation of phytoplankton carbon concentrating mechanisms during low CO_2 glacial periods and implications for the phytoplankton pCO_2 proxy. *Quaternary Sci Rev*, 208, 1-20, <https://doi.org/10.1016/j.quascirev.2019.01.012>, 2019.
- van Peer, T. E. *A palaeomagnetic, astrochronological, and environmental magnetic perspective on Oligocene-Miocene climate, using drift sediments from the Northwest Atlantic Ocean*. PhD thesis, University of Southampton, <http://eprints.soton.ac.uk/id/eprint/416832>, 2017.
- 405 Wilkens, R. H., Westerhold, T., Drury, A. J., Lyle, M., Gorgas, T., & Tian, J. Revisiting the Ceara Rise, equatorial Atlantic Ocean: isotope stratigraphy of ODP Leg 154 from 0 to 5 Ma. *Clim Past*, 13(7), 779-793, <https://doi.org/10.5194/cp-13-779-2017>, 2017.
- Zeebe, R. E., & Rae, J. W. B. Equilibria, kinetics, and boron isotope partitioning in the aqueous boric acid–hydrofluoric acid system. *Chem Geol*, 550, 119693, <https://doi.org/10.1016/j.chemgeo.2020.119693>, 2020.

410